THERMOCHEMICAL EXPLORATION OF A CAVITY BASED SUPERSONIC COMBUSTOR WITH LIQUID KEROSENE FUEL

P. Manna*, Ramesh Behera* and Debasis Chakraborty*

Abstract

Thermochemical exploration of a liquid hydrocarbon fueled scram jet combustor is presented. Three dimensional Navier Stokes equations alongwith K-ε turbulence model and single step kerosene-air reaction kinetics are solved using commercial software. Various combustor configurations with different fuel injection cavities are analyzed. Simulations capture all the essential features of the flow field. Good comparisons between computational and experimental surface pressure form the basis for further analysis. Parametric studies have been carried out with different droplet diameters to study its effect in the flow development. The numerical simulation also confirmed the experimental observation that the threshold value of length-to-depth ratio for cavity characterization is different for reacting and non-reacting flows.

***Keywords**: scramjet, cavity, liquid injection, upstream interaction*

Notation

A = coefficient matrix
A_{ebu}, B_{ebu} = combustion model constants
C_μ,$C_{\varepsilon 1}$,$C_{\varepsilon 2}$= turbulence model constants
d = particle diameter
h = cavity depth, also heat transfer coefficient
H = enthalpy
K = turbulent kinetic energy
L = length of the cavity, also latent heat of vaporization of fuel
m = mass of particle
P = pressure
Pr = Prandtl number
q = heat flux
R = residue, also mixing rate of combustion model
s = stoichiometric ratio
S = sutherland constant
S_K, S_ε = source terms for K and ε
t = time
T = temperature
u = velocity
x, y, z = coordinate axes
Y = mass fraction
Z = species mass fraction

Greek Letters

ρ = density
τ = shear stress
ε = turbulent kinetic energy dissipation rate
μ = viscosity
σ_K,σ_ε,σ_c = coefficients for K, ε and Z equations
λ = thermal conductivity
γ = ratio of specific heats

Suffix

i, j, k = axial direction
edm = eddy dissipation model
f = fuel
p = combustion products, also particle
l = laminar
t = turbulent
o = oxidiser, also stagnation value
ref = reference value

Introduction

Energy density and handling issues have rendered liquid hydrocarbon an attractive candidate as fuel for the

* Computational Combustion Dynamics Division, Directorate of Computational Dynamics, Defence Research and Development Laboratory (DRDL), Kanchanbagh Post, Hyderabad-500 058, India; Email : debasis_drdl@yahoo.co.in
Manuscript received on 26 Apr 2007; Paper reviewed, revised and accepted on 02 Aug 2007

scramjet engine in a lower atmospheric flight regime ($M \leq 8$) in volume limited applications. In a comprehensive review on scramjet technologies over past two decades, Curran [1] has identified two scramjet applications, namely, (a) hydrogen fueled engines for access to space and (b) hydrocarbon fueled engines for air launched missiles. Issues related to hypersonic inlet, isolators, liquid fuels, wall fuel injection, axial fuel injection, combustor, and nozzle of the liquid fuel scramjet have been reviewed extensively by Waltrup [2]. However, the realization of liquid hydrocarbon fueled scramjet engines would require a number of important issues viz., long ignition delay, quick vaporization and deeper penetration etc to be resolved. Deeper penetration of fuel into air stream is required for better mixing which is the key to sustained combustion. Considerable efforts have been focused on different injection schemes for different geometrical configuration and flow conditions in the past two decades. Issues related to liquid hydrocarbon fuel injection in supersonic cross flow and effective flame holding mechanism continued to be active research topics [3-11] and cavity based integrated configuration, including fuel injectors and flame holder, has been shown to possess a great potential to achieve active flame stabilization in supersonic combustor. Liquid fuel can be injected at the floor of the cavity or upstream. With a cavity, a high temperature, low speed recirculation zone can be established to serve as a pilot flame, which in turn can reduce the bulk ignition delay time and sustain a stable combustion. Furthermore, wall injection can greatly simplify the design of the combustor and cooling system as compared to the instream devices. Recently, Yu et.al [12-14] conducted a series of experimental investigations in a liquid kerosene fueled cavity based scramjet combustor with vitiated air stream having Mach no, stagnation temperature and stagnation pressure in the range of 2.5, 800-2100 K and 0.7-1.3 MPa respectively and studied various open and closed cavities. Both liquid and effervescent atomization was considered and the mixing and combustion characteristics of the combustor were explored. Various diagnostic techniques like Direct Photography, Schlieren Imaging and Planar Laser Induced Fluorescence (PLIF) imaging of OH radicals were utilized to examine the cavity characteristics. The detailed measurements of surface pressure with different cavity configurations presented in the studies are of great importance in validating any CFD code.

The physical mechanisms involved in cavity based flameholder on supersonic combustor are quiet complex and not properly understood. The existing definition of open and closed cavity characteristics is based on nonreacting flows and subject to revision for reacting flow situations. Efforts are continuing [8] to understand the stable and unstable characteristics of the cavity flow with an emphasis on the phenomena of flow induced cavity resonance. It is generally recognized that open cavities ($L/h < 10$) could be used for flame holding while the mixing enhancement could be achieved through the closed cavities.

With the advent of powerful computer, robust numerical algorithm, Computational Fluid Dynamics (CFD) techniques are routinely used in the design and analysis of scramjet propulsion system. To accurately model scramjet flow field, CFD must adequately resolve several complex physical processes including: three-dimensional shock-boundary layer interaction, turbulent mixing of high speed subsonic and supersonic streams and kinetics of hydrocarbon fuels. Although, a large volume of literature exists on numerical simulation of hydrogen combustion in scramjet combustor, the numerical simulation of hydrocarbon combustion in scramjet is comparatively small, mostly, because of complexity of modeling hydrocarbon fuel. Majority of the simulation work on hydrocarbon combustion in scramjet propulsion system is limited to relatively simple fuel. Carson et. al [15] have numerically studied ethylene combustion in a backward facing stepped scramjet combustor using a single step chemical kinetics. Their parametric studies with two different step heights (3.2 mm and 6.4 mm) reveals that the lower step height does not necessarily ensure better efficiency. Abdel-Salam et. al [16] have used FLUENT Software to study the flow field of Scramjet Combustor with both hydrogen and ethylene fuel. Rajasekharan and Babu [17] has simulated kerosene combustion in a dual mode supersonic combustor with single step chemistry and Spalart-Allmaras turbulence model using Fluent software and obtained good match with experimentally measured surface pressure. Baurle and Eklund [18] have studied cavity based scramjet combustor with ethylene fuel using VULCAN [19] Navier Stokes solver. Turbulence is modeled with Menter's SST [20] model while a 3 step 6 species reduced model is employed to describe the, chemical kinetics. Two-flight conditions corresponding to flight Mach numbers of 4.0 and 6.5 are simulated to address the problem of dual mode ramjet-scramjet operation. The computed results are shown to be very sensitive to the modeled level of heat and mass transfer. Dufour and Bouchez [21] have numerically simulated the scramjet experiment [22] with kerosene fuel using a three-dimensional Navier Stokes solver and single step chemical kinetics. A reasonable good match is obtained between the computed and experi-

mentally measured wall static pressure. It proceeds from the results that the pressure recovery and combustion efficiency can be predicted confidently from the simulation. These computations confirmed that, for the specific injector design investigated, the combustion efficiency is limited by an imperfect mixing between fuel and air.

It is clear from the above discussion that the numerical simulations of the cavity based scramjet combustor have mostly addressed the prediction of global parameters of the flow field. A scrutiny of the thermochemical parameters of the reacting flow field, particularly, in the cavity region should be carried out in sufficient detail to understand the cavity characteristics in supersonic combustion environment. In this work, the experimental conditions of the liquid atomization of kerosene fuel in a model cavity based scramjet combustor [12-13] are simulated numerically using a commercial three-dimensional reacting N-S software. The computed surface pressure of the combustor geometry with three different cavity configurations were compared with the experimental measured values and the insights of the flow characteristics of cavity based scramjet combustor is obtained through the analysis of various flow parameters.

Experimental Set-up for Which the Computations are Carried Out

The schematic of cavity based scramjet combustor experiment [12-14] for which the computations are carried out is shown in Fig.1. The combustor has rectangular cross section with an entry of 51 x 70 mm^2. The length of the combustors is 1070 mm and consists of four sections, including removable constant cross section isolator of 70 mm length, a nearly constant area section (1° divergence for boundary layer corrections) of 334 mm length (Section-I) and two expansion sections. The first expansion section (Section II) has 322 mm length with 3° divergence, whereas, the 4° divergence has been given within the length of 344 mm in the second expansion section (Section III). The test facility can supply the vitiated air to the combustor at Mach 2.5, with stagnation pressure and temperature in the range of 0.7-1.3 MPa and 800-2100 K respectively. The combustor is fitted with flush mounted interchangeable cavity modules on the top and bottom wall of the combustor. Different types of integrated wall injector cavity configuration were designed and tested at various stagnation conditions with liquid and effervescent atomization. In the present work, numerical investigations are carried out with three different cavity configurations. The depth of the cavities is 12 mm whereas the lengths of the cavities are 88, 61 and 95 mm gives the L/h ratio of 7.33, 5.08 and 7.92 respectively. The schematic of the cavity configurations with injection locations is also shown in Fig. 1. Kerosene was injected normally to the vitiated air stream via five orifices of 0.6 mm diameter. The geometrical dimension of the combustors, cavities and the injection parameters are shown in Table-1. For cavity module A, fuel is injected upstream of cavity at an

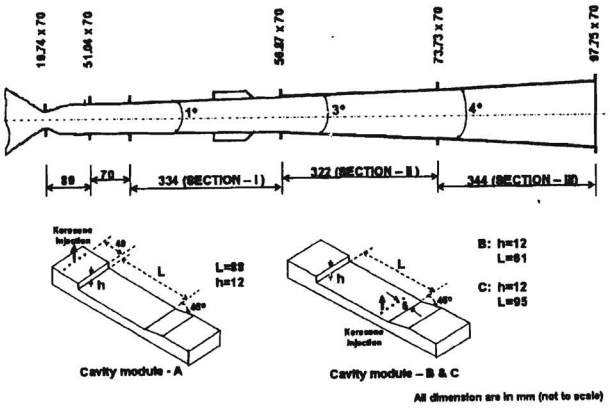

Fig.1 Experimental set-up with various cavity modules

Table-1 : Geometrical dimension of the combustors

	Config.A	Config.B	Config.C
Length (mm)	1070	1095	1095
Isolator (mm)	70	0	0
Section-I (mm)	334	275	275
Section-II (mm)	322	420	420
Section-III (mm)	344	400	400
Cavity location from combustor entry (mm)	283	145	145
Cavity depth, *h* (mm)	12	12	12
Cavity length, *L* (mm)	88	61	95
Kerosene injection region and location from inlet (mm)	Upstream of cavity 283	In cavity 201	In cavity 235
Aft ramp angle of cavity	45°	45°	45°
Fuel equvalence ratio	0.45	0.45	0.78
Vitiated air total pressure, P_0 (bar)	10.44	10.44	10.44
Vitiated air total temperature, T_0 (K)	1840	1840	1840

equivalence ration of 0.45, while for the cavity B and C, the fuel injected at the floor of the cavity at the equivalence ratio of 0.45 and 0.78 respectively. More detailed descriptions of the experiments are available in Ref.12-14.

Methodology

The software used in the present study, is a three dimensional Navier Stokes code -CFX-TASCflow [23] which is an integrated software system capable of solving diverse and complex multidimensional fluid flow problems. The code is fully implicit, finite volume method with finite element based discretisation of geometry. The method retains much of the geometric flexibility of finite element methods as well as the important conservation properties of the finite volume method. It utilizes numerical upwind schemes to ensure global convergence of mass, momentum, energy and species. It implements a general non-orthogonal, structured, boundary fitted grids. In the present study, the descretisation of the convective terms are done by upwind difference scheme and K-ε model with wall functions is used to model turbulence. The details of the formulation are given in the theory documentation of Ref. [23]. The governing equations and modeling of various physical processes used in the simulation are described in the following subsections.

Governing Equations

The appropriate system of equations governing the turbulent flow of a compressible gas may be written as:

Continuity equation:

$$\frac{\partial \rho}{\partial t}+\frac{\partial}{\partial x_k}\left(\rho u_k\right)=0 \quad k=1,2,3$$

Momentum equation:

$$\frac{\partial}{\partial t}\left(\rho u_i\right)+\frac{\partial}{\partial x_k}\left(\rho u_i u_k\right)+\frac{\partial P}{\partial x_i}=\frac{\partial(\tau_{ik})}{\partial x_k}, \quad i,k=1,2,3$$

Energy equation:

$$\frac{\partial}{\partial t}(\rho H)+\frac{\partial}{\partial x_k}\left(\rho u_k H\right)=-\frac{\partial}{\partial x_k}\left(u_j \tau_{jk}\right)+\frac{\partial q_k}{\partial x_k}, \quad j,k=1,2,3$$

Turbulent kinetic energy (K) equation :

$$\frac{\partial}{\partial t}(\rho K)+\frac{\partial}{\partial x_k}(\rho u_k K)=\frac{\partial}{\partial x_k}\left(\left(\frac{\mu_l}{\mathrm{Pr}}+\frac{\mu_t}{\sigma_K}\right)\frac{\partial K}{\partial x_k}\right)+S_K$$

Rate of dissipation of turbulent kinetic energy (ε) equation:

$$\frac{\partial}{\partial t}(\rho \varepsilon)+\frac{\partial}{\partial x_k}(\rho u_k \varepsilon)=\frac{\partial}{\partial x_k}\left(\left(\frac{\mu_l}{\mathrm{Pr}}+\frac{\mu_t}{\sigma_\varepsilon}\right)\frac{\partial \varepsilon}{\partial x_k}\right)+S_\varepsilon$$

Species mass fraction (Z):

$$\frac{\partial}{\partial t}(\rho Z)+\frac{\partial}{\partial x_k}(\rho u_k Z)=\frac{\partial}{\partial x_k}\left(\left(\frac{\mu_l}{\mathrm{Pr}}+\frac{\mu_t}{\sigma_c}\right)\frac{\partial Z}{\partial x_k}\right)$$

where, ρ , u_i , p , H are the density, velocity components, pressure and total energy respectively and $\mu=\mu_l+\mu_t$ is the total viscosity; μ_l , μ_t being the laminar and turbulent veicosity anbd Pr is the Prandtl number. The source terms S_k and S_ε of the K and ε equation are defined as,

$$S_K=\tau_{ik}\frac{\partial u_i}{\partial x_k}-\rho\varepsilon \quad \text{and} \quad S_\varepsilon=C_{\varepsilon 1}\tau_{ik}\frac{\partial u_i}{\partial x_k}-C_{\varepsilon 2}\frac{\rho\varepsilon^2}{K}$$

where turbulent shear stress is defined as

$$\tau_{ik}=\mu_t\left(\frac{\partial u_i}{\partial x_k}+\frac{\partial u_k}{\partial x_i}\right)$$

Laminar viscosity (μ_l) is calculated from Sutherland law as

$$\mu_l=\mu_{ref}\left(\frac{T}{T_{ref}}\right)^{3/2}\left(\frac{T_{ref}+S}{T+S}\right)$$

where, T is the temperature and μ_{ref}, T_{ref} and S are known coefficient. The turbulent viscosity μ_t is calculated as

$$\mu_t=C_\mu\frac{\rho K^2}{\varepsilon}$$

The coefficients involved in the calculation of μ_t are taken as

$$C_\mu=0.09, \quad C_{\varepsilon 1}=1.44, \quad C_{\varepsilon 2}=1.92$$
$$\sigma_K=1.0, \quad \sigma_\varepsilon=1.3, \quad \sigma_c=0.9$$

The heat flux q_k is calculated as $q_k=-\lambda\frac{\partial T}{\partial x_k}$, λ is the thermal conductivity

Combustion Modeling

For combustion, the eddy dissipation combustion model is used for its simplicity and robust performance in predicting reactive flows. The eddy dissipation model is based on the concept that chemical reaction is fast relative to the transport process in the flow. When reactants mix at the molecular level they instantaneously form products. The model assumes that the reaction rate may be related directly to the time required to mix reactants at molecular level. In turbulent flows, this mixing time is dictated by the eddy properties and therefore the burning rate is proportional to the rate at which turbulent kinetic energy is dissipated i.e., reaction rate $\alpha\ \varepsilon/K$, where K is the turbulent kinetic energy and ε is its rate of dissipation. The chemistry of the combustion reaction is represented on a molar basis by $C_{12}H_{23} + 17.75O_2 = 12CO_2 + 11.5H_2O$. The mixing rate determined from the Eddy Dissipation Model (EDM) is given as.

$$R_{k,\,edm} = -A_{ebu}\ \bar{\rho}\ \frac{\varepsilon}{K}\ \min\left\{Y_f, \frac{Y_o}{r_s}, B_{ebu}\frac{Y_p}{1+r_s}\right\}$$

where, Y_f, Y_o and are the mass fractions of fuel, oxidizer and products respectively, A_{ebu} are the model constants and r_s is the stoichiometric ratio.

Discrete Phase Model

Lagrangian tracking method is used for discrete phase model to characterize the flow behaviour of the dispersed phase fluid (kerosene liquid). The prediction of flows involving the dispersed phase involves the separate calculation of each phase with source terms generated to account for the interaction between the phases. The flow of the continuous phase is predicted using a discretized form of the Navier Stokes equations. With the dispersed phase there is no continuum and each particle interacts with the fluid and other particles discretely. Therefore, the most widely applied method available to determine the behaviour of the dispersed phase is to track several individual particles through the flow field. Each particle represents a sample of particles that follow an identical path. The behaviour of the tracked particles is used to describe the average behaviour of the dispersed phase. Only viscous drag on the particles is considered in the study. Particle-particle interactions and effect of turbulence in the discrete phase is not modulated in the analysis.

Source Terms for the Governing Equations

For the purpose of describing the types of sources generated by particles, it is convenient to consider the differences between inert and reacting particles. Both inert and reacting components of particles exchange momentum with the fluid due to viscous drag and exchange energy due to particle heating. Reacting particles may also exchange mass with the fluid as well as exchange momentum and energy due to mass sources. If the sources are grouped according to inert components (those sources common to all particle types) and reacting components (those sources only found with reacting particles) then particle sources may be generalized as shown in Table-2.

Discretisation of Governing Equations

The CFX-TASCflow solver utilizes a finite volume approach, in which the conservation equations in differential form are integrated over a control volume described around a node, to obtain an integral equation. The pressure integral terms in the momentum integral equation and the spatial derivative terms in the integral equations are evaluated using finite element approach. An element is described with eight neighboring nodes. The advective term is evaluated using upwind differencing with physical advection correction. The set of discretised equations form a set of algebraic equations: $A\ \vec{x} = b$ where $\vec{x}$ is the solution vector. The solver uses an iterative procedure to update an approximated x_n (solution of x at n^{th} time level) by solving for an approximate correction x' from the equation $A\ \vec{x'} = \vec{R}$, where $\vec{R} = \vec{b} - A\vec{x_n}$ is the residual at n^{th} time level. The equation $A\ \vec{x'} = \vec{R}$ is solved approximately using an approach called Incomplete Lower Upper factorization method. An algebraic multigrid method is implemented to reduce low frequency errors in the solution of the algebraic equations. Maximum residual $\left(= \phi_j^{n+1} - f(\phi_j^{n+1}, \phi_j^n) < 10^{-4}\right)$ is taken as convergence criteria.

Results and Discussions

The schematic of the scramjet combustor is given in Fig. 1. Three different cavity configurations were simulated. The geometrical details of the cavity and the operating conditions of the simulations are summarized in Table-1. The cavity module A and B are operating with the fuel equivalence ratio of 0.45 while the operating equivalence ratio of cavity module C is 0.78.

Table-2 : Source terms of the governing equations

Source	Inert component	Reacting component
Mass	------	$\dot{N}\,\delta m_p$
Momentum	$\dot{N} m_p (v_p - v_f)\left[1 - \exp\left(\frac{-18\mu\delta t}{\rho d^2}\right)\right]$	$\dot{N}\,\delta m_p v_p$
Energy	$\dot{N}\int_0^{\partial t} h_c A_p (T_f - T_p)\, dt$	$\dot{N}(-L_v \delta m_v + Q_c \delta m_c)$

δt = time step over which sources are applied

$\dot{N}$ = number of particles injected per unit time along the path

δm_p = mass loss of a particle in time step, δt

h_c = convective heat transfer coefficient per unit area, A_p

$L_v \delta m_v$ = energy required to vaporize volatiles of mass, δm_v

$Q_c \delta m_c$ = energy generated in burning char of mass, δm_c

T_p , T_f = particle and fluid temperature

ρ , μ , d = density, viscosity, and diameter of particle respectively

v_f, v_p = fluid and particle velocity

In order to consider a realistic boundary layer of the combustor entry, the computational domain has been taken from throat of the facility nozzle. Taking advantage of the symmetry in the geometry, only 1/4th of the combustor is considered for simulation. A total number of 354 x 30 x 16 structured grids are used along the length, height and width of combustor respectively. The grids are fine near the injection holes, walls and the cavity region, while relatively coarser grids are provided in the remaining portion of the combustor. In the simulation, X-axis is taken along the length of the combustor while Y and Z axes are along the height and width of the combustor respectively. The origin is placed at the throat center of the facility nozzle. As the computational domain starts from the throat of the facility nozzle, sonic conditions are applied in the inflow plane. No slip and adiabatic wall boundary conditions are imposed at the wall, while symmetric and supersonic outflow boundary conditions are applied at the symmetry plane and outflow boundary respectively. Yu et. al [12] has measured the kerosene droplet diameter in the kerosene sprays with different injector diameters using a Malvern particle sizer and found that the droplet diameter is about 20 μm for the injector diameter of 0.4 to 0.6 μm. It was also observed that in the injecting pressure range of 2.1 to 4.5 MPa, the dependence of droplet size on the injecting pressure was quiet insignificant. In the simulation, Sauter Mean Diameter (SMD) of the kerosene droplet is taken as 20 μm.

The grid independence of the solution is established by carrying out the nonreacting simulation with two different grids of size 354 x 30 x 16 and 425 x 35 x 18 and comparing the wall pressure at side wall between these grids in Fig. 2. It is very clear from the figure that by changing grids from 0.17 million to 0.27 million, the results do not change appreciably thus demonstrating that the present grid is adequate to capture the essential features of the solutions.

The qualitative features of the flow field in the combustor are depicted through the comparison of various important thermochemical parameters for reacting and non-reacting cases of the cavity module A. The Mach number distribution in the symmetry plane of the combustor is compared between reacting and non-reacting cases in Fig. 3. The Mach number in the non-reacting cases is predominantly supersonic. While for reacting case, the Mach number reduces significantly due to heat release. The flow field accelerates again in the downstream direction because of divergence in the combustor. The cross sectional view of the Mach number distribution at various axial stations (X = throat, combustor inlet = 0.0, 0.1, 0.2, 0.3, 0.4, 0.5, 0.65, 0.85 and exit =1.07 m) is shown in

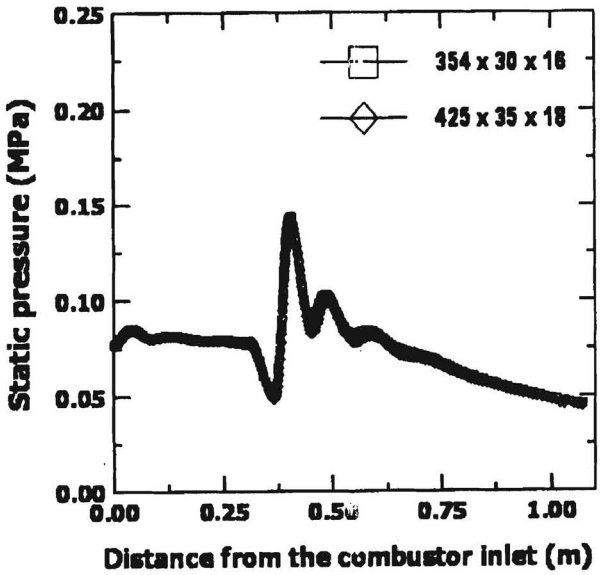

Fig.2 Grid independence study, cavity module-A

Fig.3 Mach no. in vertical symmetry plane

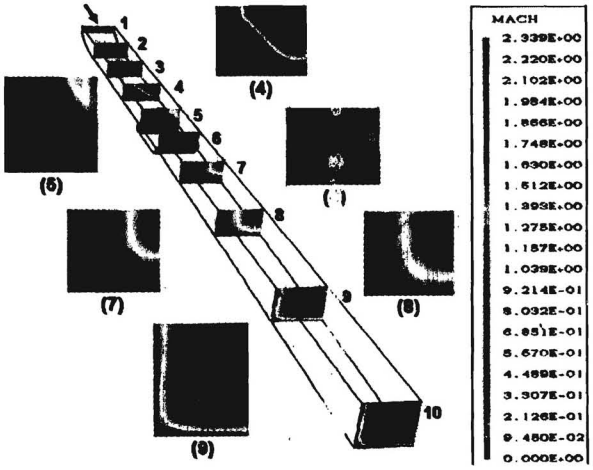

Fig.4 Mach no. in different axial planes
X=throat(1), combustor inlet=0(2), 0.1(3), 0.2(4), 0.3(5), 0.4(6), 0.5(7), 0.65(8), 0.85(9) and exit=1.07 m(10)

Fig.4. The wall injection has resulted in significant upstream interaction and caused a massive separation in the sidewall of the combustor. The separation bubble is extended upto 136mm upstream of the injection point as seen from the cross sectional view of axial velocity at different longitudinal locations near the injection plane presented in Fig.5. Only negative values of the axial velocity component is plotted to show the region of separation. The cross sectional views of the mass fraction of CO_2 - the reaction product are presented in Fig. 6 to depict the zone covered by reaction. Although, the kerosene is injected at 49mm upstream of the cavity, the presence of CO_2 is seen

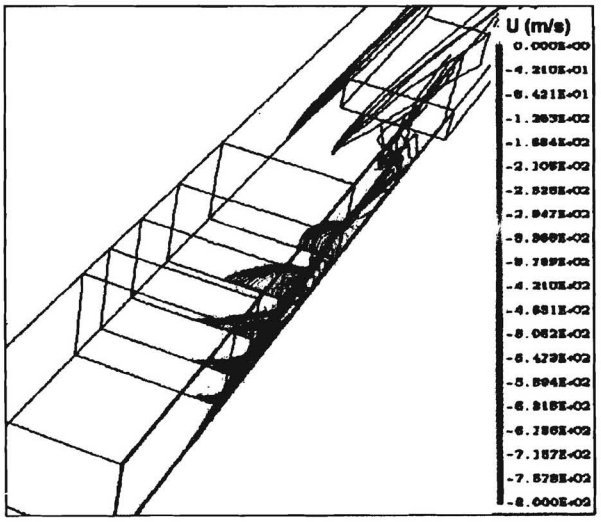

Fig.5 Axial velocity profile at different axial locations upstream of injection

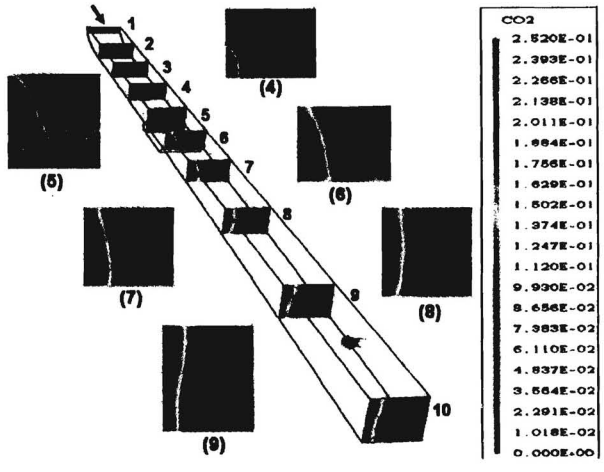

Fig.6 CO_2 mass fraction in different axial planes
X=throat(1), combustor inlet=0(2), 0.1(3), 0.2(4), 0.3(5), 0.4(6), 0.5(7), 0.65(8), 0.85(9) and exit=1.07 m(10)

at 136mm upstream of the injection point as the fuel has diffused through the recirculation separation bubble. Although, CO_2 has covered complete width of the cross section, reaction is not very intensive. This is mainly because of relatively low equivalence ratio of 0.45. Significant quantity of oxygen is still remaining to be burnt in the core of the combustor, which can be clearly seen in the cross sectional view of the O_2 mass fraction presented in Fig.7. The liquid kerosene is seen to vaporize completely within 543mm of distance from the inlet of the combustor. The computed side wall surface pressure for the three cavity configurations (A,B,C) are shown in Fig. 8(a) to 8(c). As mentioned earlier, the equivalence ratios of cavity A and cavity B configurations are 0.45, whereas the equivalence ratio for cavity C is 0.78. The surface pressure for the non-reacting case for the cavity configuration is also shown in Fig.8(a). The increase in static pressure starts much upstream of injection location showing significant upstream interaction due to heat release. The static pressure was seen to reach an approximately isobaric plateau in the nearly constant area section X = 250mm and decrease continuously till the combustor exit because of flow expansion in the divergent section of the combustor. A good comparison with experiment and computational values are obtained except in the region of fuel injection where the computations have shown a higher value. The higher heat release caused due to fast chemistry assumption in the simulation is conjectured to be the cause of higher surface pressure in the injection zone. In the divergent portion, the principle thrust producing element of the combustor, the agreement between the two is very good. Although, for the cavity module B and C, the computations predict the upstream interaction i.e. the location of pressure increase reasonably well, the computed pressure rise for cavity module A is slightly downstream. It is to be noted that for cavity module A fuel is injected from the combustor wall upstream of the cavity in supersonic flow in contrast to the injection in cavity flow for module B and C where the flow is subsonic. The injection of the liquid fuel in supersonic flow in cavity module A has caused much severe upstream interaction compared to the cavity injection in configuration B although the fuel equivalence ratio is the same. The prediction of the upstream separation for the cross-flow injection in supersonic flow is very challenging. Various researchers [24-26] have reported problems in predicting these upstream separation even for unconfined flow. A very fine mesh in the vicinity of the injection zone may be required to resolve these differences which have not been attempted in this study. The difference between the surface pressure for the non-reacting and reacting cases presented for the cavity module A in Fig. 8(a) quantifies the effect of heat release in the surface pressure of the combustor. The side wall surface pressure distribution for the equivalence ratio of 0.45 between the three configurations is compared in Fig. 9. The difference in the injection pattern and the cavity geometry in three configurations have caused different heat release pattern and hence different pressure distribution. Also, minor differences exist between the three combustor geometries. A 70mm isolator is provided in the combustor configuration A, while the isolator is not present for configuration B and C. The

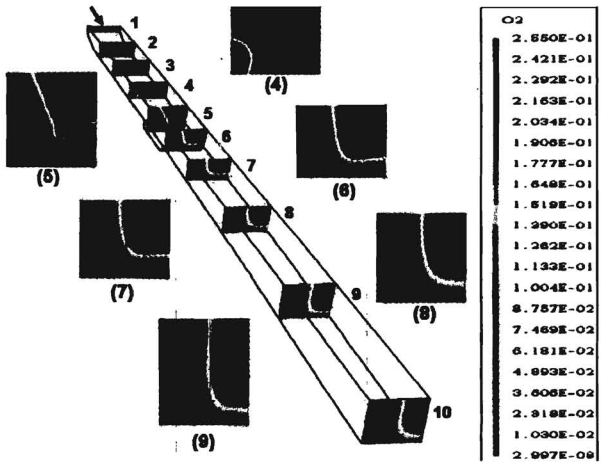

Fig.7 O_2 mass fraction in different axial planes X=throat(1), combustor inlet=0(2), 0.1(3), 0.2(4), 0.3(5), 0.4(6), 0.5(7), 0.65(8), 0.85(9) and exit=1.07 m(10)

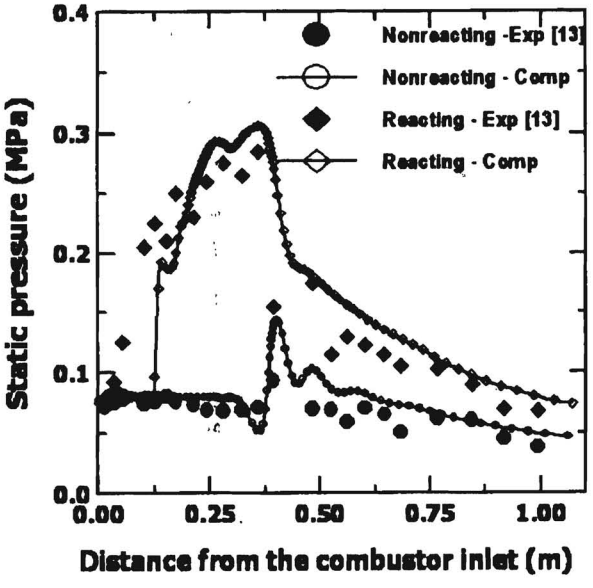

Fig.8a Side wall surface pressure comparison for cavity module-A, ϕ = 0.45

length of various sections of the combustor is also different. All the geometrical details have been provided in Table-1. For configuration A, fuel is injected in the upstream of cavities while configurations B and C the fuel injection is done in the cavity floor. The comparison of the area averaged parameters namely Mach number, static pressure and static temperature in the combustor is shown in Fig.10(a) to 10(c). The computed combustion efficiencies for these three configurations for equivalence ratio 0.45 are shown in Fig.11. The efficiency has been estimated as the ratio between the actual CO_2 formed to the maximum possible CO_2 which can be formed in case of complete burning. The computed combustion efficiency is quiet high as the fuel equivalence ratio is relatively

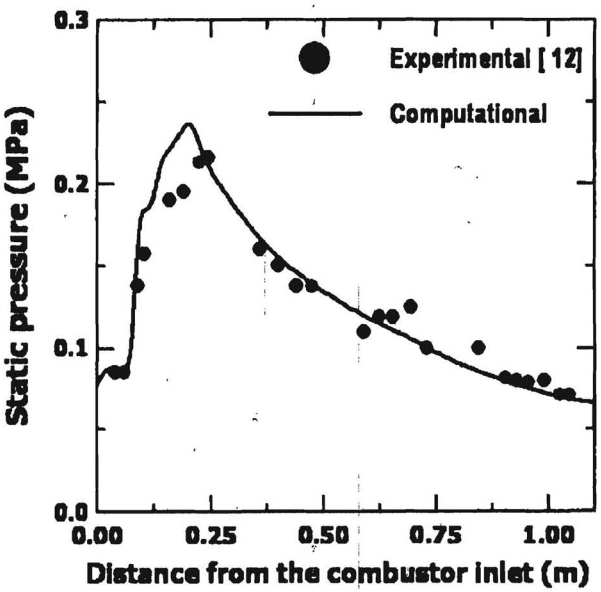

Fig.8b Side wall surface pressure comparison for cavity module-B, ϕ = 0.45

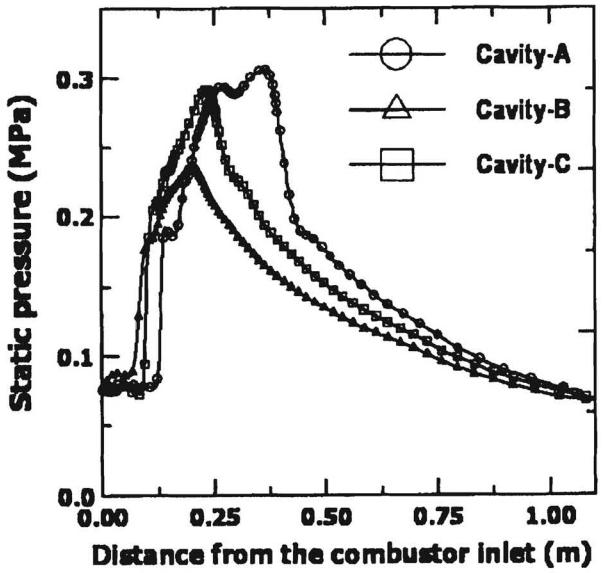

Fig.9 Side wall surface pressure comparison for cavity module-A, B and C, ϕ = 0.45

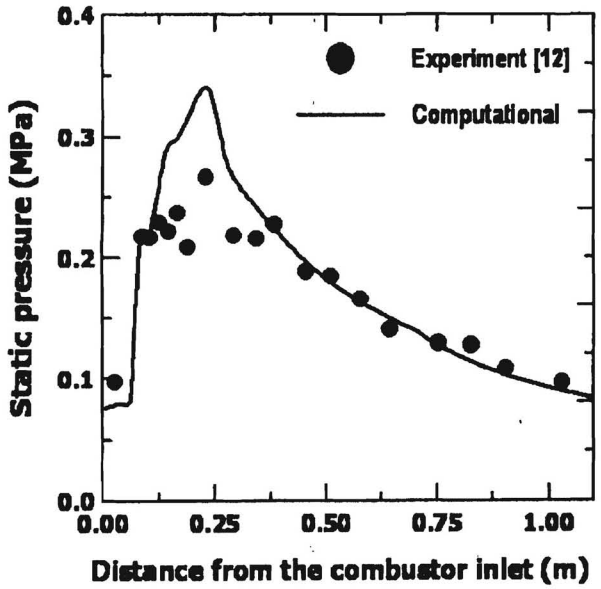

Fig.8c Side wall surface pressure comparison for cavity module-C, ϕ = 0.78

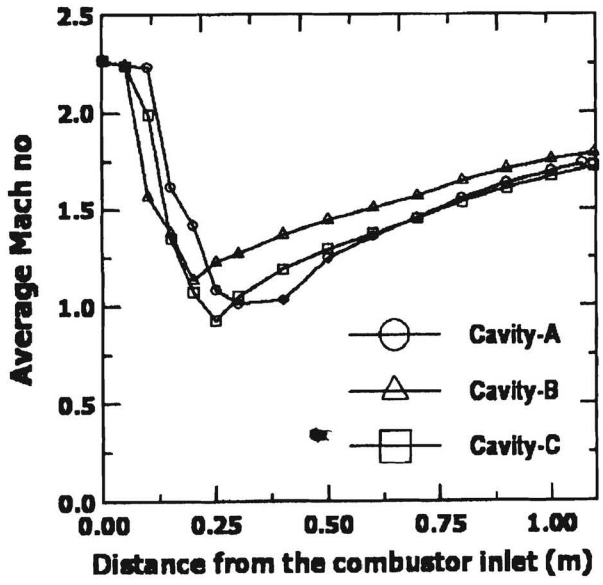

Fig.10a Comparison of average Mach no.

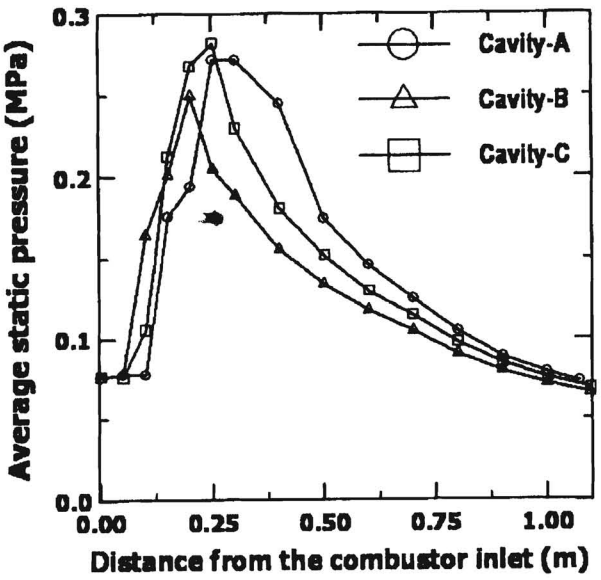

Fig.10b Comparison of average static pressure

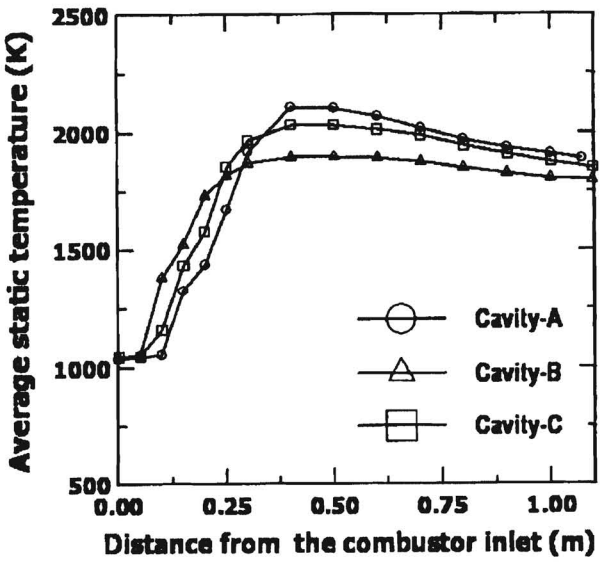

Fig.10c Comparison of average static temperature

small. For configuration A, complete combustion has been observed within 600mm distance. The computed thrusts for these three cases are presented in Table-3.

It is observed that due to graded heat release, the combustion efficiency in cavity module A is more than other two cavity modules which makes it superior from combustion characteristics point of view. However, the achieved thrust from this configuration is not maximum. This may be due to loss incurred by the big separation

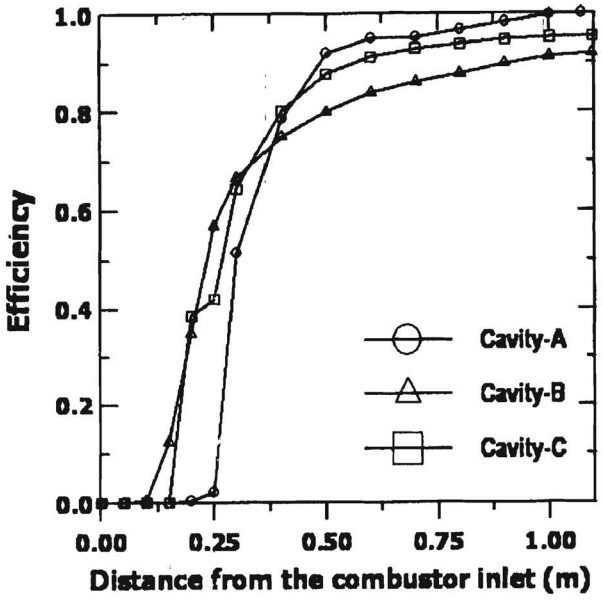

Fig.11 Comparison of combustion efficiency

Table-3 : Thrust availability from various configurations

Configuration	Thrust (N)
Combustor - A	596.4
Combustor - B	596.0
Combustor - C	605.2

bubble ahead of injection point. Although, cavity configuration C gives maximum thrust compared to other configurations, the heat release has caused the area averaged Mach number less than unity.

To study the effect of three-dimensionality in the flow field, the surface pressures in the side wall and the top walls of the configuration A for equivalence ratio 0.45 are compared with the area averaged pressure in Fig.12. It is observed that the circumferential variation of the surface pressure extends upto 400 mm and three-dimensionality reduces significantly in the downstream direction. The computed surface pressure for configuration B for the equivalence ratios of 0.45 and 0.78 is compared in Fig.13 to show the effect of equivalence ratio on the surface pressure. Both the surface pressure and upstream interactions have increased for the higher equivalence ratio. The effect of droplet diameter on the surface pressure was determined by carrying out the simulation with the different particle diameters of 1, 5, 10 and 20 μm for the cavity

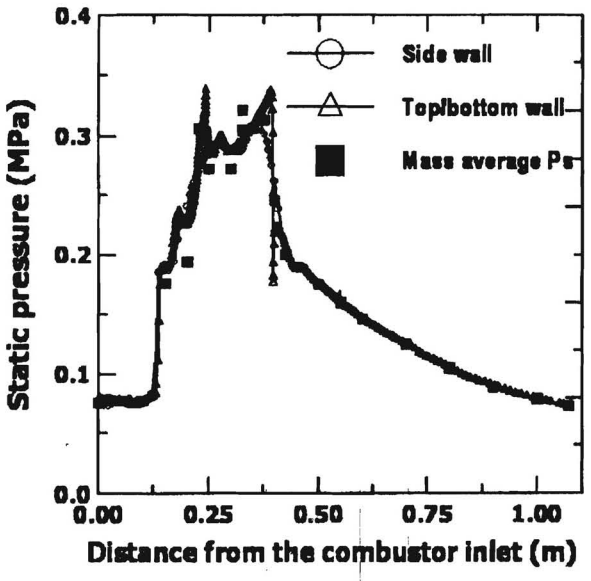

Fig.12 Comparison of wall pressure for cavity module-A, ϕ = 0.45

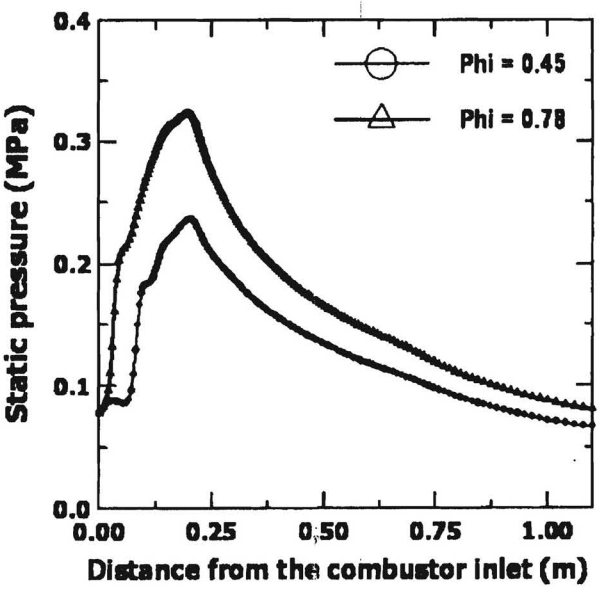

Fig.13 Side wall surface pressure comparison for various equivalence ratio for cavity module-B

module A configuration with equivalence ratio 0.45. The computed surface pressures with the different droplet diameters are compared with experimental values in Fig.14. It can be observed that with lesser droplet diameter, the evaporation is faster and heat release is intensive. This has lead to surface pressure to rise near the injection zone. The higher heat release is also responsible for more upstream interaction for the lesser droplet diameter case.

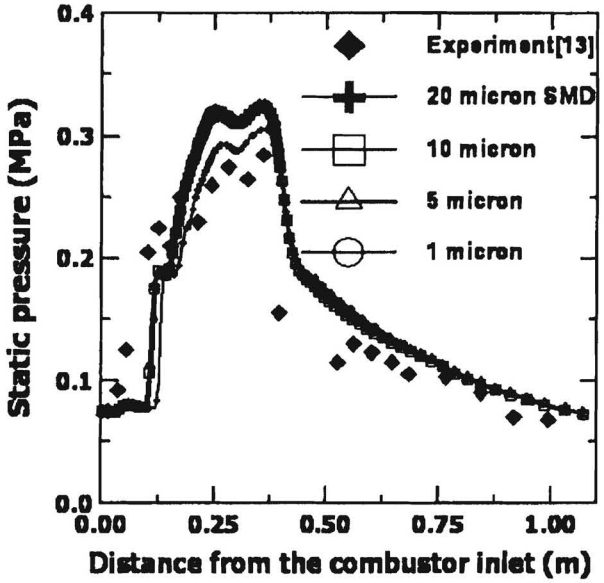

Fig.14 Comparison of surface pressure to see the effect of particle sizing for cavity module-A, ϕ = 0.45

The effect of the droplet diameter on the surface pressure is insignificant in the divergent portion of the combustor.

In the present simulation L/h ratio of the cavities are in the range of 5.42 - 7.92 and according to the definition [6, 9] these cavities must be considered as open. Self-sustaining pressure oscillation could be observed in the open cavities due to the shear layer impingement in the rear wall of the cavity. The threshold value of L/h ratio defining the cavity characteristics is based on non-reacting flows. Burnes et. al [6] observed that the flow induced resonance is suppressed by fuel injection in the cavity. Additionally, the combustion of kerosene inside the cavity changes the flow field very significantly. The flow patterns inside the cavity considered in these simulations are shown in Fig.15 through the streak line plot alongwith the negative axial velocity. The non- reacting flow pattern in cavity A, is also included in the figure to show the change of the flow pattern between the reacting and non-reacting flow. The Shear layer for non-reacting flow in cavity A is attaching in the rear wall while the shear layer for the reacting flows are impinging on floor of the cavity thus exhibiting the closed nature of the cavities for the reacting flow. Yu et. al [12] also observed from their experimental investigation, the threshold value of the length-to-height ratio defining close cavity should be no more than 5 to 7 for reacting flows. Cross sectional view of the temperature distribution at various axial locations in the cavities are shown in Fig.16 for reacting flow in three cavity configurations. It can be observed that there exists a high tempera-

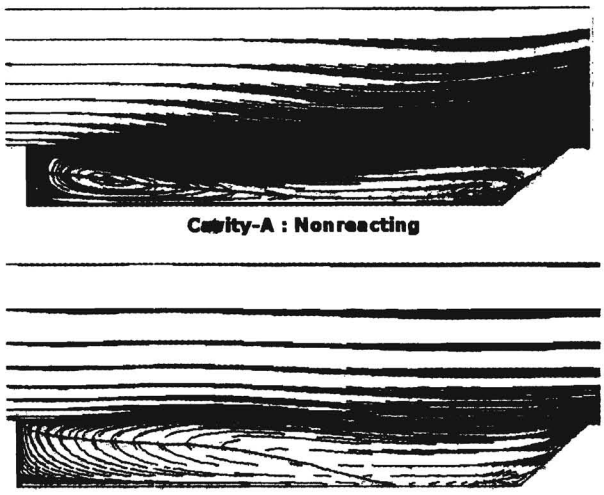

Fig.15 Flow pattern inside the cavity

ture region in the cavity to produce hot pool for sustaining kerosene combustion. This is also a characteristic of the closed cavity. The numerical simulation also confirmed the important conclusion drawn by Yu et. al [12] to determine the threshold value of L/h to define the cavity characteristics in the reacting flow.

Conclusions

Numerical simulations are carried out to understand the flow phenomena in a cavity based scramjet combustor with liquid kerosene fuel. Three dimensional Navier Stokes equations along with K-ε turbulence model and single step kerosene-air kinetics are solved using a commercial CFD software. Reacting and nonreacting flow fields are investigated for three different combustor configurations with different fuel injection cavities. Good comparison of surface pressure is obtained between experimental and numerical values except in the injection region for different equivalence ratios in the range of 0.45 to 0.78. Heat release due to reaction has caused significant upstream interactions and fuel diffused upstream through the separation bubble. The predicted location of the start of the pressure rise (upstream interaction) matches well when the fuel is injected in the cavity floor. For the case of injection in the combustor wall ahead of the cavity, the computed location of pressure rise is in the downstream location compared to the experimental value. The parametric studies with different fuel droplet diameters indicate that the upstream interaction and pressure rise is more intensive near the injection zone for the droplet with lesser diameter. The effect is not very significant in the downstream region. The comparisons of the cavity flow fields

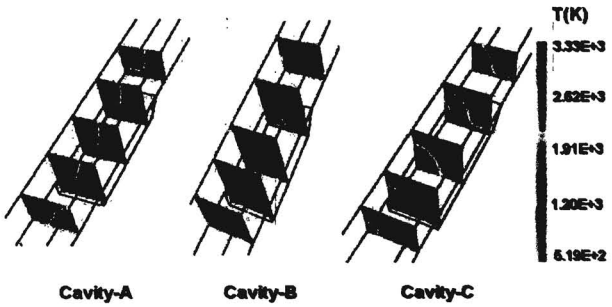

Fig.16 Temperature distribution in cavity

between reacting and nonreacting cases show that the existing definition of the cavity characteristics needs modification for reacting flow. Present study also confirms the experimental observation that the length-to-height ratio defining close cavity should be no more than 5 to 7 for reacting flows.

References

1. Curran, E. T., "Scramjet Engines: The First Forty Years", Journal of Propulsion and Power, Vol.17, No.6, 2001, pp.1138-1148.

2. Waltrup, P.J., "Liquid-fueled Supersonic Combustion Ramjet: A Research Perspective", Journal of Propulsion and Power, Vol.3, No.6, 1987, pp.515-524.

3. Anrashkov, V., Burunovsky, S. and Levin, V., "Gas Dynamic Features of Supersonic Combustion in a Model Combustion Chamber", AIAA Paper 90-5268, 1990.

4. Mathur, T., Gruber, M., Jackson, K., Donbar, J., Donaldson, W., Jackson, T. and Billig, F., "Supersonic Combustion Experiments with a Cavity-based Fuel Injector", Journal of Propulsion and Power, Vol.17, No.6, 2001, pp.1305-1312.

5. Li, J.G., Yu, G., Zhang, X.Y. and Huary, Q.S., "Combustion of Kerosene in a Supersonic Stream", AIAA Paper 2000-0615, 2000.

6. Burnes, R., Parr, T.P., Wilson, K.J. and Yu, K., "Investigation of Supersonic Mixing Control Using Cavities - Effects of Fuel Injection Location", AIAA Paper 2000-3618, 2000.

7. Owens, M.G., Tehranian, S., Segal, C. and Vinogradov, V., "Flame Holding Configuration for Kerosene

Combustion in a Mach 1.8 Airflow", Journal of Propulsion and Power, Vol.14, No.4, 1998, pp.456-461.

8. Yu, K., Wilson, K.J. and Schadow, K.C., "Effect of Flame Holding on Supersonic - Combustion Performance", Journal of Propulsion and Power, Vol.17, No.6, 2001, pp.1287-1295.

9. Hsu, K.Y., Carter, C., Crafton, J., Gruber, M., Donbar, J., Mathur, T., Schommer, D. and Terry, W., "Fuel-distribution about a Cavity Flame-holder in Supersonic Flow", AIAA Paper 2000-3585, 2000.

10. Gruber, M.R., Donbar, J.M., Carter, C.D. and Hsu, K.Y., "Mixing and Combustion Studies using Cavity-based Flame Holders in a Supersonic Flow", Journal of Propulsion and Power,Vol.20, No.5, 2004, pp. 769- 778.

11. Vinogradov, V.A., Kobigsky, S.A. and Petrov, M.D., "Experimental Investigation of Kerosene Fuel Combustion in Supersonic Flow", Journal of Propulsion and Power, Vol.11, No.1, 1995, pp.130-134.

12. Yu, G., Li, J.G., Chang, X.Y., Chen, L.H. and Sung, C.J., "Investigation of Kerosene Combustion Characteristics with Pilot Hydrogen in Model Supersonic Combustors", Journal of Propulsion and Power, Vol.17, No.6, 2001, pp.1263-1272.

13. Yu, G., Li, J.G., Chang, X.Y., Chen, L.H. and Sung, C.J., "Fuel Injection and Flame Stabilization in Liquid - Kerosene Fueled Supersonic Combustor", Journal of Propulsion and Power, Vol.19, No.5, 2003, pp.885-893.

14. Yu, G., Li, J.G., Chang, X. Y., Chen, L.H. and Sung C.J., "An Experimental Study of Kerosene Combustion in a Supersonic Model Combustor using Efferscent Atomization", Proceedings of 30th International Symposium of Combustion, 2005, pp.2859 -2816.

15. Carson, R.A., Mohieldin, T.O. and Tiwari, S., "Numerical Study of Hydrogen and Ethylene Injected Normally in a Two Dimensional Dual-mode Scramjet Combustor", AIAA Paper 2004-1035, 2004.

16. Abdel-Salam, T., Tiwari, S. and Mohieldin, T .O., "Study of Supersonic Combustion Characteristics in a Scramjet Combustor", AIAA Paper 2003-3550, 2003.

17. Rajasekharan, A. and Babu, V, "Numerical Simulation of Kerosene Combustion in a Dual Mode Supersonic Combustor", AIAA Paper 2006-5041, 2006.

18. Baurle, R.A. and Eklund, D.R., "Analysis of Dual-mode Hydrocarbon Scramjet Operation of Mach 4-6.5", Journal of Propulsion and Power, Vol.18, No.5, 2002, pp.990-1002.

19. White, J.A. and Morrison, J.H., "A Pseudo Temporal Multigrid Relaxation Scheme for Solving ParabolizedNavier Stokes Equation", AIAA Paper 1999-3360, 1999.

20. Menter, F.R., "Two Equation Eddy-viscosity Turbulence Models for Engineering Applications",AIAA Journal, Vol.32, No.8, 1994, pp.1598-1605.

21. Dufour, E. and Bouchez, M., "Computational Analysis of a Kerosene Fueled Scramjet", AIAA Paper 2001-1817, 2001.

22. Bouchez, M., Dufour, E. and Montazel, X., "Hydrocarbon Fueled Scramjet for Hypersonic Vehicles", AIAA Paper 1998-1589, 1998.

23. CFX-TASCflow Computational Fluid Dynamics Software, Version 2.11.1, AEA Technology Engineering Software Ltd, 2001.

24. Sriram, A. and Mathew, J., "Numerical Prediction of Two-dimensional Transverse Injection Flows", AIAA Paper 2004-1099, 2004.

25. Rizzetta, D.P., "Numerical Simulation of Slot Injection into Turbulent Supersonic Stream", AIAA Journal, Vol.30, No.10, 1992, pp.2434-2439.

26. Viti, V., Wallis, S., Schetz, J.A., Neel, R. and Bowersox, R.D.W., "Jet Interaction with a Primary Jet and an Array of Smaller Jets", AIAA Journal. Vol.42, No.7, 2004, pp.1358-1368.